# Climatic Changes of the Last 18,000 Years: Observations and Model Simulations

COHMAP MEMBERS*

**Changes in solar radiation arising from changes in the orientation of the earth's axis had pronounced effects on tropical monsoons and mid-latitude climates as well as on ice-sheet configuration during the last 18,000 years. COHMAP (Cooperative Holocene Mapping Project) has assembled a global array of well-dated paleoclimatic data and used general-circulation models to identify and evaluate causes and mechanisms of climatic change. For the northern tropics, particularly in Africa and Asia, data and model results show that the orbitally induced increase in solar radiation in summer 12,000 to 6,000 years ago enhanced the thermal contrast between land and sea and thus produced strong summer monsoons, which raised lake levels in regions that are arid today. In middle to high latitudes the climatic response to both the insolation changes and to the retreating ice sheets led to readjustments in the vegetation in both the Northern and Southern hemispheres. Model results show that the large North American ice sheet split the westerly jet stream into northern and southern branches over North America. An increase in storms associated with the southern branch helps explain high lake levels and increased woodlands in the southwestern United States during full-glacial conditions. Comparisons of paleoclimatic data with the model simulations are important because models provide a theoretical framework for evaluating mechanisms of climatic change, and such comparisons help to evaluate the potential of general circulation models for predicting future climates.**

THE LARGE CHANGES IN THE EARTH'S CLIMATE DURING THE last 18,000 years have altered the vegetation, ice volume, and sea-surface conditions over most of the globe. Ice sheets and some desert lakes disappeared, vegetation was drastically altered, many types of large mammals became extinct, and agriculture was developed, which changed the course of human history. The nature and timing of these changes have posed many puzzles to scientists studying Quaternary climate. Why were lake levels high in the American Southwest during the glacial maximum at 18 ka (thousand years ago) and low in the Northwest at the same time, and were these variations in lake levels a result of changes in seasonal precipitation or temperature? Why were lakes in the Sahara expanded during the early Holocene (12 to 6 ka), when virtually all the American desert basins were dry? Why were summer temperatures warmest in central North America at 6 ka, when the summer radiation maximum was at 9 to 11 ka? What combination of climatic variables can explain the faunal and floral assemblages of the last glacial period that have no modern analogs, and what caused the changing patterns of vegetation in America and Europe during and after the retreat of the ice sheets?

Global climate has long been postulated as a key factor influencing each of these regional changes, but until recently we were uncertain about both the causes of the global climate changes and the regional interconnections among key components of the global climate system. Climatologists had discounted the role of the earth's orbital variations, the full climatic impact of the ice sheets was not understood, and climate models were not well enough developed to test the potential influence of these and other factors.

Oxygen isotope studies of ocean sediment cores helped to remove some uncertainties about Quaternary environmental changes. Periodicities in the data indicated that the driving force behind much long-term climatic change is the varying insolation at the top of the atmosphere (*1–3*). Orbitally induced variations in insolation are the "pacemaker" of the ice ages (*4*). CLIMAP (*5*) used a diverse array of marine and continental indicators to reconstruct conditions at the earth's surface at 18 ka, a time when earlier insolation changes had contributed to the growth of large ice sheets in the Northern Hemisphere. This reconstruction was the basis for experiments with improved climate models to reconstruct the general atmospheric circulation for the glacial maximum (*6*).

COHMAP (Cooperative Holocene Mapping Project) has continued the CLIMAP strategy of using both geologic data and models to investigate the global and regional dynamics of climate change. Focusing on the sequence of changes during the last 18,000 years, COHMAP researchers have assembled data that provide geologic records of spatial and temporal changes in climate from radiocarbon-dated stratigraphic sequences from several continents and oceans. These data have been systematically compared with the model simulations of past climates (*7–13*) (Fig. 1). The central goal of COHMAP research is an improved understanding of the physics of the climate system, particularly the response of tropical monsoons and mid-latitude climates to orbitally induced changes in solar radiation and to changing glacial-age boundary conditions, such as ice-sheet size. In this article we describe the research design and some key results from COHMAP research that help answer the

*The authors are P. M. Anderson, C. W. Barnosky, P. J. Bartlein, P. J. Behling, L. Brubaker, E. J. Cushing, J. Dodson, B. Dworetsky, P. J. Guetter, S. P. Harrison, B. Huntley, J. E. Kutzbach, V. Markgraf, R. Marvel, M. S. McGlone, A. Mix, N. T. Moar, J. Morley, R. A. Perrott, G. M. Peterson, W. L. Prell, I. C. Prentice, J. C. Ritchie, N. Roberts, W. F. Ruddiman, M. J. Salinger, W. G. Spaulding, F. A. Street-Perrott, R. S. Thompson, P. K. Wang, T. Webb III, M. G. Winkler, and H. E. Wright, Jr.

COHMAP is a multi-institutional consortium of scientists studying late Quaternary environmental changes as recorded in geologic data and simulated by numerical models. Correspondence should be directed to J. E. Kutzbach, Center for Climatic Research, University of Wisconsin, 1225 West Dayton Street, Madison, WI 53706; T. Webb III, Department of Geological Sciences, Brown University, Providence, RI 02912; or H. E. Wright, Jr., Limnological Research Center, University of Minnesota, Minneapolis, MN 55455.

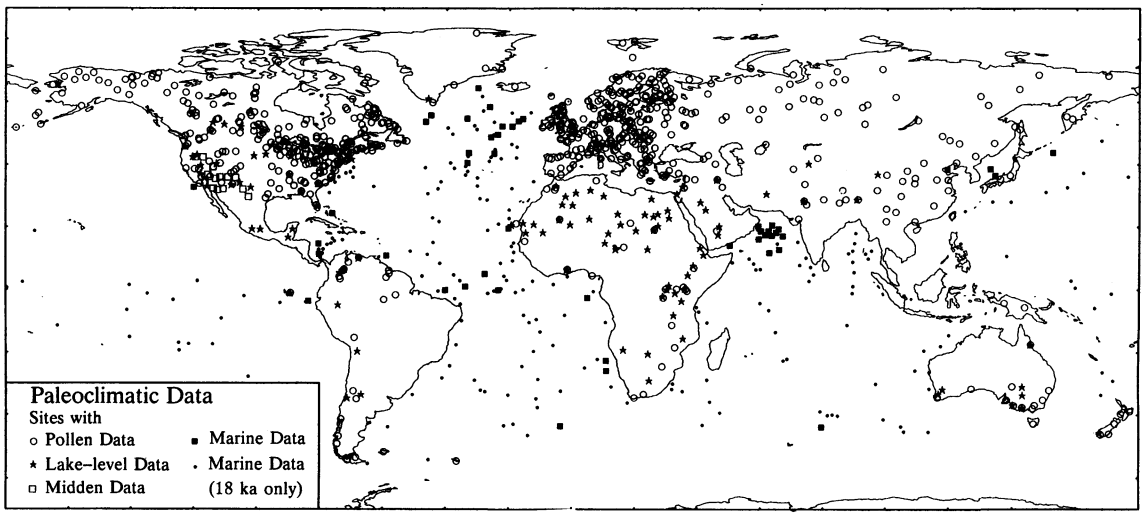


**Fig. 1.** Location of sites in the COHMAP global paleoclimate database. Pollen data for each core were entered for specified intervals back to 18,000 years ago: at approximately 300-year intervals for North America, 500-year intervals for Europe, 3000-year intervals elsewhere. Lake-level data were entered for each 1000-year interval, and marine plankton for each 3000-year interval. Radiocarbon-dated plant-macrofossil assemblages from pack rat middens were entered in 3000-year intervals. The location of CLIMAP (*5*) marine plankton records for 18 ka are also indicated.

questions posed in the introductory paragraph.

Comparisons of reconstructed paleoclimates with model simulations provide a way to evaluate mechanisms of climate change. They also test the ability of models to simulate the very different climates of the past. The ability to simulate a range of climates is important because the same mathematical models are being used to study the effects of the anthropogenic increase of $CO_2$ and to predict future changes in climate.

## Design of Paleoclimatic Experiments

Until about 15 years ago, most theoretical work concerning past climates was derived from conceptual models of climatic change and involved either qualitative reasoning from simple models or interpretation of the geologic record. The recent development of general-circulation models for the atmosphere and oceans has permitted quantitative paleoclimate modeling and thus led to a major advance in theoretical studies. These mathematical models are based on nonlinear flow equations and the principles of mass and energy conservation. With the advent of supercomputers, climate modelers are able to make the large numerical calculations required for paleoclimate studies (*14–19*) in a reasonable time.

The COHMAP simulation experiments were made with the Community Climate Model (CCM) of the National Center for Atmospheric Research (NCAR) (*20*). As input to this model we prescribed the orbitally determined insolation, mountain and ice-sheet orography, atmospheric trace-gas concentrations, sea-surface temperatures, sea-ice limits, snow cover, albedo, and effective soil moisture (*7, 21–30*).

Changes in the seasonal and latitudinal distribution of solar radiation are produced by changes in three aspects of earth-sun geometry. The 22,000-year precession cycle regulates the time of year when the earth-sun distance is a maximum or minimum and hence affects seasonality. The 40,000-year tilt cycle, in which the inclination of the earth's axis varies about 1.5° on either side of its present value of about 23.5°, affects the latitudinal distribution of solar radiation. The third aspect, very long period changes in the eccentricity of the earth's orbit, is discussed elsewhere (*31*). The possible effects of these orbital variations on climate were studied by Croll more than 100 years ago and by Milankovitch in the early 1900s (*1*).

The boundary conditions chosen by COHMAP are schematically shown in Fig. 2. The seasonal and latitudinal distributions of solar radiation at 18 ka were similar to those of today; therefore, the atmospheric conditions simulated for glacial times must be attributed primarily to altered surface boundary conditions. Between 15 and 9 ka, the earth-sun distance decreased in northern summer and the axial tilt increased; therefore, the seasonality of climate increased in the Northern Hemisphere and decreased in the Southern Hemisphere. As a result, continental ice sheets and sea ice retreated and the oceans warmed. At about 9 ka average solar radiation over the Northern Hemisphere was 8% higher in July and 8% lower in January than it is today. After 9 ka these seasonal radiation extremes decreased toward modern values.

The various boundary conditions were the basis for a sequence of model experiments in which the model provided "snapshots" of the temperature, precipitation, sea-level pressure, and winds for selected dates during the past 18,000 years (Figs. 2, 3, and 4) (*25*). Differences among the model results for these times show how changes in orbital forcing and surface boundary conditions may have contributed to the observed climatic record (*28*).

An atmospheric general circulation model is a highly sophisticated tool for illustrating some of the climatic consequences of the changes in solar radiation and surface boundary conditions. It can be used to demonstrate the link between changes in widely different places and to identify the physical mechanisms through which changed boundary conditions alter climate. In these ways the model simulations provide possible explanations for the climatic changes evident at a continental and global scale. At the same time discrepancies between the model results and the paleoclimatic data reveal the need for new research to improve the model physics, the boundary conditions, the geologic data, and the methods used to infer climatic information from the data.

## Paleoclimatic Data

Three main types of biologic and geologic data were chosen that could provide quantitative or semiquantitative estimates of paleoclimate over subcontinental areas (Fig. 1). They are pollen, lake levels, and marine plankton. These types of data have traditionally been used to construct conceptual models of climatic change, but are used here for comparisons with the model results.

*Pollen.* Lake sediments contain pollen that represents the local and

regional vegetation. Over broad regions, the relative abundance of each pollen type reflects the distribution of its source taxon. Through time, variations in pollen abundance reflect variations in such climatic variables as summer and winter temperature and annual moisture. The network of pollen records, particularly in eastern North America and western Eurasia, permits mapping of the broad-scale changes in vegetational associations as the ice sheets retreated and atmospheric circulation changed (*9, 10*).

*Lake levels.* Under certain conditions, lakes act as natural rain gauges. Closed-basin lakes are sensitive to the balance between precipitation and evaporation, which is directly linked to atmospheric circulation (*32*). Regionally synchronous changes in past lake levels, as reconstructed from a variety of geomorphic, sedimentologic, paleoecologic, and archeologic evidence, thus reflect regional changes in effective moisture (precipitation minus evaporation). Lake-level records are particularly valuable for paleoclimatic interpretations in the arid regions of Africa, Australia, and the western United States because the pollen records in these areas are sparse; exposed paleoshorelines in many areas testify to wetter climates in the past. Changes in effective moisture and seasonality of precipitation are also inferred from other data sets, such as plant macrofossils in pack rat middens in mountainous terrain of the western United States (*33*).

*Marine plankton.* Marine plankton responds to physical and chemical variations in the surface waters of the world oceans. The distributions of many species are correlated with surface-water temperature, and large changes in assemblages occur across prominent water-mass boundaries (*34*). Plankton fossils in marine sediments thus allow us to estimate the properties and boundaries of ocean water masses of former times.

## Modeling Experiments and Paleoclimatic Reconstructions

The following sections summarize the key dynamic and thermodynamic processes of climatic change that emerged from our modeling experiments and analyses of geologic data. We focus on two geographic regions where our data coverage is best: (i) the North American–Eurasian sector (Fig. 3) and (ii) the monsoon sector and southern mid-latitudes (Fig. 4). Detailed information on both the modeling studies and the paleoclimatic data base has been published elsewhere (*7, 25, 35*). The results demonstrate that orbital changes can explain in broad terms the history of climate and landscape development from the last glacial maximum at 18 ka to the present, after allowance is made for such internal feedbacks as the adjustment of the atmospheric and oceanic circulations to the presence of ice sheets, which themselves responded to orbital forcing with a time constant of many thousands of years (*36*). Climate events of short duration were not considered in the data synthesis or in the modeling experiments.

## North American–Eurasian Sector

*Present-day conditions.* One key feature of the mid-latitude climates is the westerly jet stream aloft in winter, which marks the boundary between warm and cold air masses and governs the location and path of traveling storm systems (Fig. 3). It crosses the west coast of North America at about 50°N. Inland it turns southeast and crosses the east coast at about 40°N. At the surface the Atlantic and Pacific subtropical high-pressure cells dominate summer circulation, and the Aleutian and Icelandic lows prevail in winter over the northern oceans. The NCAR CCM simulates accurately the modern location and intensity of these circulation features. The simulation of the modern fields of temperature and precipitation is not perfect, but in most areas and seasons the differences between the model results and the observed climate are small relative to changes simulated in the paleoclimate experiments.

Permanent land ice is restricted mainly to Greenland. Sea ice covers much of the Arctic Ocean in summer as well as winter (Fig. 3). Spruce-dominated forest extends throughout the boreal zone from Alaska to Labrador and across northern Eurasia, and it covers high-elevation areas farther south on both continents. Temperate regions in eastern North America and western and southern Europe have broad-leaved deciduous forests, typically containing oak. The American Southwest is dry, with few lakes in the intermontane basins. Polar conditions occur in the northwestern North Atlantic, as shown by the abundance of the foraminifer *Neogloboquadrina (Globigerina) pachyderma* (left-coiling) and by clastic detritus dropped from icebergs and sea ice. Subtropical conditions, indicated by *Globigerinoides ruber* (white and pink varieties), extend from Florida to northern Africa.

*Dynamics of the model simulations.* At 18 ka the different boundary conditions include ice sheets at their maxima, with winter sea ice in the North Atlantic extending south to the coast of France (Fig. 3). South of the sea-ice border in both the North Atlantic and the North Pacific, prescribed sea-surface temperatures were as much as 10°C lower than those at present. Simulated temperatures over the land were also much lower than at present, especially over the elevated and highly reflective ice sheets. Strong anticyclonic circulation around the Laurentide ice sheet brought cold conditions to the North Atlantic and strong easterly winds along the southern flank of the ice sheet. The sharp temperature gradient at the southern edge of the continental ice sheets and the extensive sea ice field was

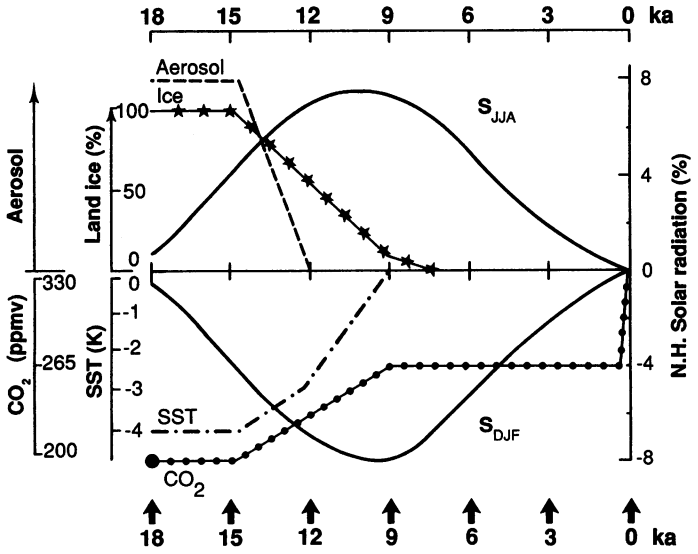


**Fig. 2.** Boundary conditions for the COHMAP simulation with the Community Climate Model for the last 18 ka (thousand years ago). External forcing is shown for Northern Hemisphere solar radiation in June through August ($S_{JJA}$) and December through February ($S_{DJF}$) as percent difference from the radiation at present. Internal boundary conditions include land ice (Ice) as percent of 18 ka ice volume (*5, 7, 70*), global mean annual sea-surface temperatures (SST) as departures from present (*5, 7*), excess glacial-age aerosol (Aerosol) with arbitrary scale (*71*), and atmospheric $CO_2$ concentration ($CO_2$) in parts per million by volume (*72*). The arrows mark the times of the seven sets of simulation experiments. The one for 18 ka included the lowered $CO_2$ concentration (200 ppmv, large filled circle); the others had the $CO_2$ concentrations of the control case (330 ppmv) rather than a stepwise increase. Experiments incorporating increased glacial-age aerosol loading have not been completed.

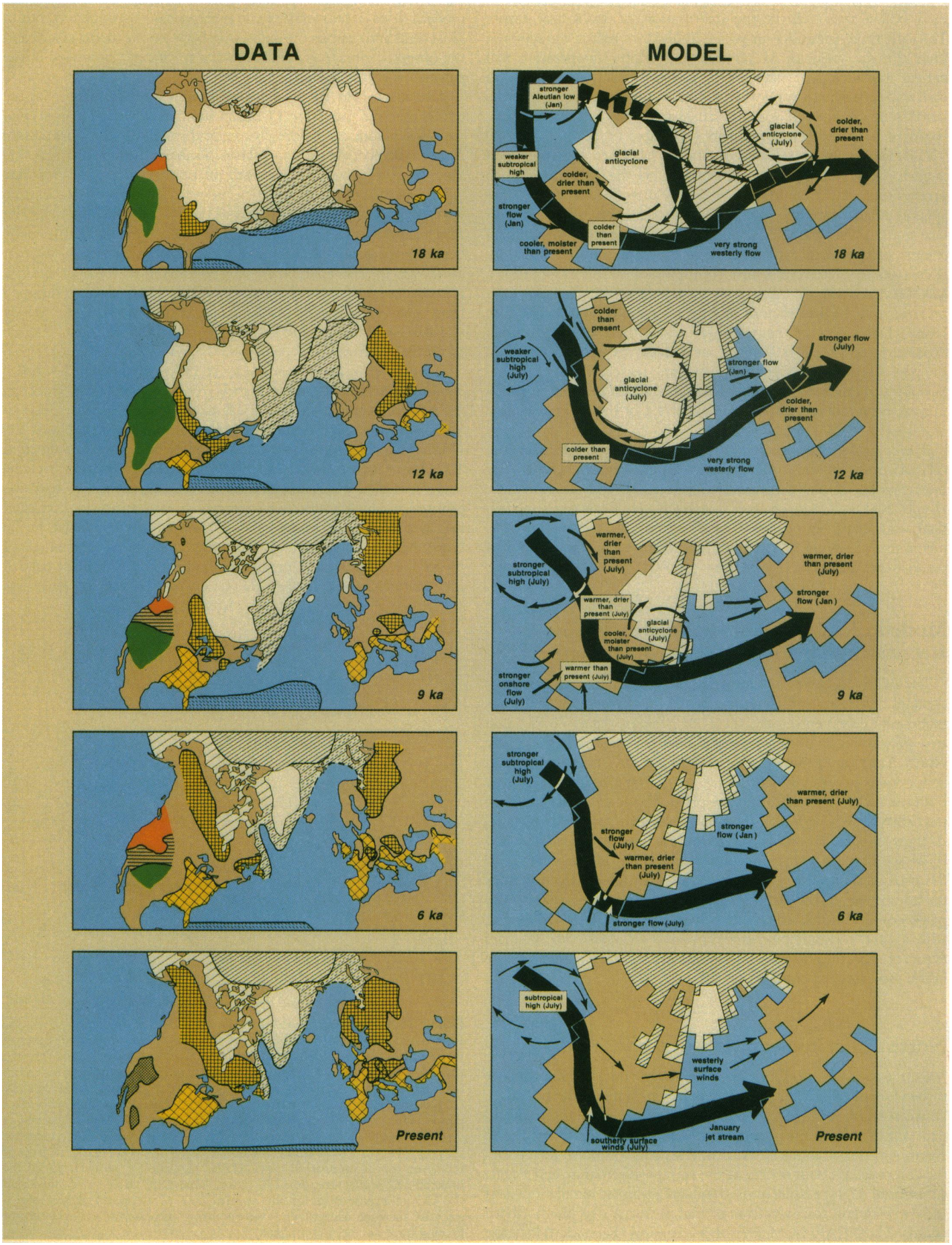
DATA
MODEL
18 ka
stronger Aleutian low (Jan)
glacial anticyclone (July)
colder, drier than present
weaker subtropical high
glacial anticyclone
colder, drier than present
stronger flow (Jan)
colder than present
cooler, moister than present
very strong westerly flow
18 ka
12 ka
colder than present
stronger flow (July)
weaker subtropical high (July)
stronger flow (Jan)
glacial anticyclone (July)
colder, drier than present
colder than present
very strong westerly flow
12 ka
9 ka
warmer, drier than present (July)
stronger subtropical high (July)
warmer, drier than present (July)
stronger flow (Jan)
warmer, drier than present (July)
glacial anticyclone (July)
cooler, moister than present (July)
warmer than present (July)
stronger onshore flow (July)
9 ka
6 ka
stronger subtropical high (July)
warmer, drier than present (July)
stronger flow (July)
stronger flow (Jan)
warmer, drier than present (July)
stronger flow (July)
6 ka
Present
subtropical high (July)
westerly surface winds
southerly surface winds (July)
January jet stream
Present

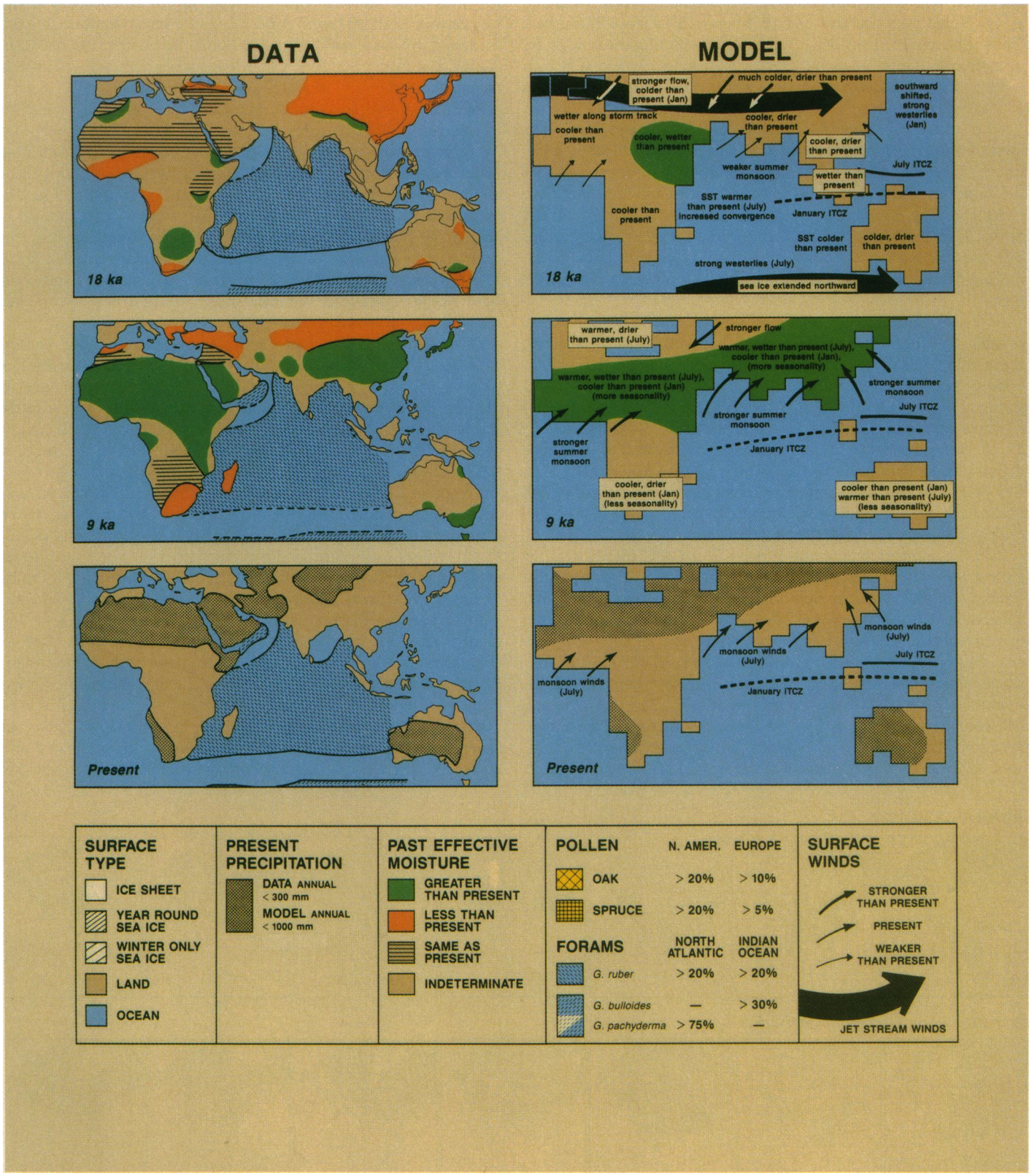


**Fig. 3** (facing page) and **Fig. 4** (above). Changes in the atmosphere, geosphere, and biosphere that accompanied the transition from glacial to interglacial conditions during the past 18,000 years, as illustrated by geologic and paleoecologic evidence (*73*) (left panels on each figure), and the highlights of the paleoclimatic simulations (right panels) (*25*). The "data" panels show the extent of ice sheets and of year-round and winter only sea ice; from 18 ka to 9 ka (thousand years ago) they show the broadened land areas resulting from lowered sea level. The distributions of oak and spruce as inferred from pollen data are shown for eastern North America and Europe. Moisture status relative to present is shown for western North America, Africa, Asia, and Australia from 18 to 6 ka. The present region where annual precipitation is less than 300 mm is shown for the southwestern United States and for Africa, Asia, and Australia. The "model" panels show the distribution of ice sheets and sea ice that served as boundary conditions for the simulations. Surface winds and the position of the jet stream as simulated by the model are shown in schematic form by arrows (broken arrows if jet is weak). For the simulation of the present climate, regions where annual precipitation is less than 1000 mm are indicated (Fig. 4 only). Comparisons noted on the simulations (for example, colder, wetter) in all cases are with reference to present conditions.

associated with a strengthened jet stream aloft, which extended across North America and east to Eurasia. The large 3-km-thick Laurentide ice sheet was also responsible for splitting the flow of the jet stream in winter across all of North America, with one branch located in southern North America and the other along the northern edge of the ice sheet.

By 12 ka the general warming of the climate associated with increased summertime solar radiation had begun, and the Laurentide ice sheet had decreased in size and thickness sufficiently so that the winter jet was no longer split, although it was still stronger than it is today. The glacial anticyclone weakened in the western United States, where westerlies replaced easterlies. The glacial anticyclone over western Europe was also weaker than it was during the glacial maximum, and the increased summer insolation warmed the continent.

At 9 ka the increased insolation in summer played a much larger role but the still smaller Laurentide ice sheet continued to influence the climate. Only a small glacial anticyclone remained active in eastern North America. By then the Pacific subtropical high had strengthened off the west coast of North America, and northwesterly winds replaced westerly winds along the coast in the Northwest. The increased insolation caused summer temperatures to be higher than at present in both Eurasia and western North America (by 2° to 4°C), but it was still colder than at present just south of the ice sheet in eastern North America. A southerly summer monsoonal flow was evident along the Gulf Coast and in Mexico.

By 6 ka summer temperatures were 2° to 4°C higher than at present throughout the continental interiors of North America and Eurasia, and the southerly flow into the eastern United States had strengthened. Strong westerlies blew in the Midwest and in Europe; they have weakened from 6 ka to the present, and summer temperatures have declined with the reduction in summertime insolation.

*Paleoclimatic data.* At 18 ka, with the ice sheets and the North Atlantic sea ice at their maximum extent (Fig. 3), *N. pachyderma* (left-coiling) was abundant far to the south of its current range. Spruce and oak forests were absent from Europe because of the cold, dry conditions, and permafrost was widespread. The Mediterranean lowlands were treeless, although lake levels in Turkey and the Levant were high. In North America, spruce forest dominated in the Midwest, subalpine parkland in the Pacific Northwest, and tundra in Alaska, but in the Southwest lake levels were high and woodlands were expanded.

After 18 ka oak in both Europe and North America, spruce in North America, and *N. pachyderma* and *G. ruber* all moved north, and by 6 ka prairies had expanded to a maximum in the American Midwest as a result of increased summer warmth. Modern plant assemblages did not form until about 10 ka (*37, 38*). After 12 ka lake levels were lower in the American Southwest than they were earlier, and in the Northwest and Alaska conditions became warmer. In Europe after 9 ka the range of spruce expanded westward from Russia to Scandinavia. After 6 ka the southern limit of spruce in both Europe and North America shifted to the south, as summer temperatures decreased (*11, 39, 40*).

*Data-model comparisons.* Patterns of change observed in the data are consistent with many of the circulation, temperature, and moisture-balance changes simulated by the model. Vegetation moved north as the ice sheets melted and temperatures increased, and greatest summer warmth occurred in western Canada much earlier than in central North America (*25, 40, 41*). The southward displacement of the jet stream and storm tracks at 18 ka explains the higher lake levels and expansion of woodlands in the American Southwest, and cold and dry conditions in the Northwest can be attributed to the easterly winds of the glacial anticyclone (*42*). Regional studies (*12, 13, 43, 44*) have demonstrated that the model simulates the general geographic patterns of selected climatic variables; the model results in turn provide useful explanations for the past patterns in the data.

In eastern North America, statistical models derived from the modern relations between pollen and climate have been used to transform the climate model results into maps of the pollen abundances for six major pollen types (*12*). The model-simulated maps for spruce from 18 ka to the present show a time sequence of patterns and changes that match those in the map sequence of observed values (Fig. 5). Comparisons show that simulated and observed patterns for most other taxa from 9 ka to present are

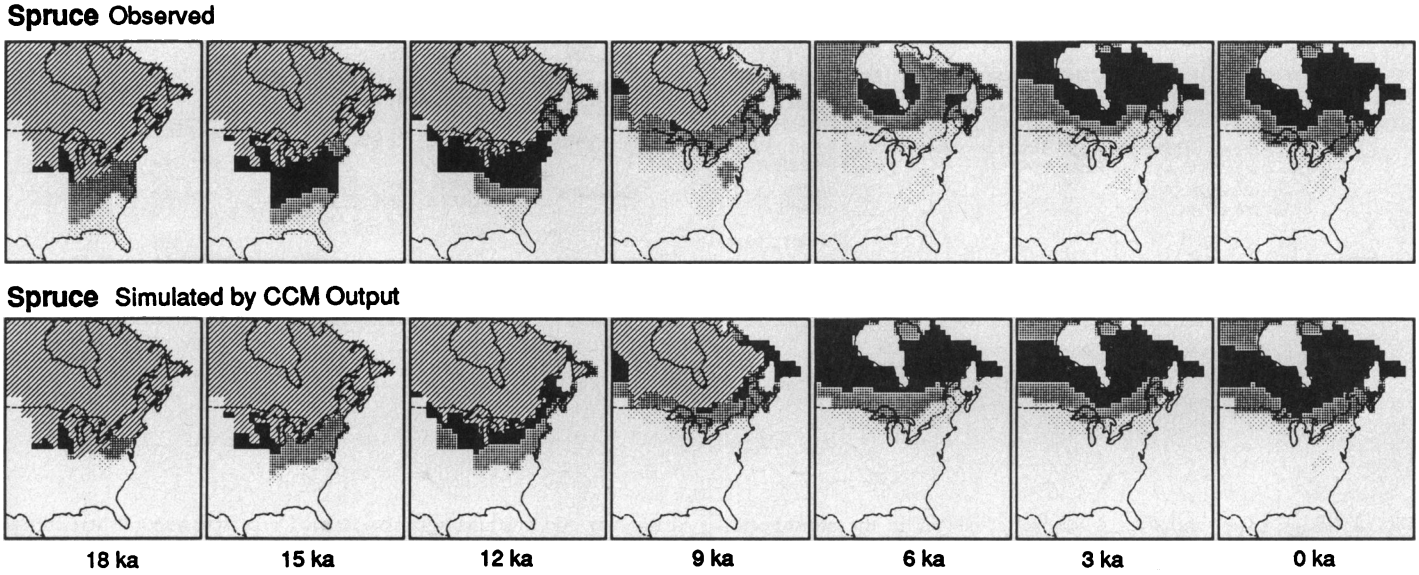


**Fig. 5.** Maps showing observed (upper row) and model-simulated (lower row) percentages of spruce pollen for each 3000-year interval from 18 ka to the present (0 ka). Region with diagonal lines in north is a digital representation of the location of the Laurentide ice sheet, which shrank in area after 18 ka (thousand years ago) and was gone soon after 6 ka. Area of spruce abundance is shown by dark stippling for >20%, intermediate stippling for 5 to 20%, and light stippling for 1 to 5% spruce pollen. Simulation values were produced by applying the observed (present) association between spruce pollen and climatic variables to the temperature and precipitation values simulated by the climate model. Fair to good agreement in mapped patterns for the observed and simulated values of spruce pollen indicate that the model simulates a combination of temperature and precipitation values compatible with the presence of spruce trees in the regions where they grew (*12*).

similar, but discrepancies are evident in the distribution of several taxa in the southeastern United States from 18 to 12 ka. For this period the model simulated July temperatures that were substantially higher than those indicated by the data. Further work is needed to understand why this discrepancy arose. The map comparisons also show that the model had only fair success in simulating precipitation patterns in the mid-latitudes (a problem with most general circulation models), but that it did simulate correctly the location of the border between prairie and forest in central North America during the past 9000 years (*9, 12*).

## Monsoon Sector and Southern Mid-Latitudes

*Present-day conditions.* The present-day northern summer–monsoon circulation is driven by the relative warmth of the African-Asian landmass compared to the surrounding ocean (*45*). Hydrostatic considerations show that this thermal gradient results in low pressure over land and high pressure over the ocean, producing southerly to southwesterly inflow of moist air and heavy monsoonal precipitation to west Africa and south and east Asia. Much of north Africa and central Asia are beyond the penetration of the monsoon rains and are hot and dry. Aloft, a large anticyclone develops, with an easterly jet on its southern flank, which stretches from the northern Indian Ocean to west Africa. The model simulates this summer monsoon circulation. Some features of the January circulation are also well simulated, although the model overestimates the strength of the cross-equatorial flow from the Northern to the Southern Hemisphere in the Atlantic sector.

Modern vegetation includes equatorial rain forest flanked to north and south by broad belts of dry forest and savanna. Subtropical deserts occur in both hemispheres because of low precipitation (Fig. 4). African lake levels are low except for a few basins close to the equator in west and east Africa. Water levels are also low in the Arabian Peninsula and low to intermediate in Afghanistan, northwest India, and central Asia. In the western Indian Ocean the modern distribution of the foraminifer *Globigerina bulloides* reflects the occurrence of coastal upwelling driven by the southwesterly summer-monsoon winds. Tropical and subtropical water masses are indicated by the distribution of *Globigerinoides ruber*. Southern Australia, New Zealand, and southern South America receive seasonally uniform or winter-dominated rainfall generated by westerly storm tracks over the southern oceans, but, at low latitudes, the subtropical high-pressure cells produce easterly tradewinds, summer monsoons, and interior or lee-side deserts.

*Dynamics of the model simulations.* At 18 ka the highly reflective ice sheets, generally cold oceans, and equatorward-extended sea-ice borders resulted in a significantly different simulated climate from what occurs today in the monsoon region and the southern mid-latitudes (Fig. 4). The low temperatures produced by these boundary conditions strengthened the north-south temperature gradient over Eurasia and thereby helped to displace the wintertime polar front and the westerlies southward to parts of northwest Africa, the Mediterranean, and southern Asia. The circumantarctic sea-ice boundary at 18 ka lay about 7° latitude closer to the equator than at present (*5*), and the resulting steeper temperature gradient strengthened the southern westerlies, especially across the Indian and the South Pacific oceans.

The tropics were slightly cooler than they are at present, but most regions had rainfall similar to present levels or were slightly drier. The simulation of wetter conditions than those today in East Africa and drier conditions in south Asia for 18 ka was caused in part by the warmer-than-present waters of the western equatorial Indian Ocean (*46*), as specified by CLIMAP (*5*). These warm waters may reflect an altered global pattern of glacial-age ocean currents (*29*).

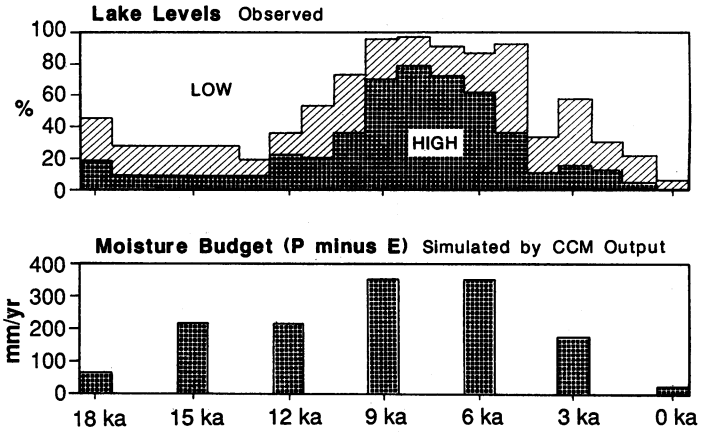


**Fig. 6.** Observed status of lake levels (upper row) and model-simulated moisture budget, precipitation-minus-evaporation (lower row), for each 1000 years (observations) or each 3000-year interval (model) from 18 ka (thousand years ago) to present (0 ka). The temporal variations in percentage of lakes with low, intermediate, or high levels is taken from the Oxford lake-level data bank. The observations and the simulated hydrologic budgets from the climate model (CCM) are for the latitude belt 8.9° to 26.6°N (*8*). The observations and simulations agree in placing the highest lake levels and largest excess of precipitation over evaporation in the interval 9 to 6 ka.

The increase in July and decrease in January insolation between 12 and 6 ka (Figs. 2 and 4) produced a major strengthening of northern monsoons. The north African–Eurasian landmass was 2° to 4°C warmer than at present, and the enhanced land-ocean thermal contrast and strengthened monsoons brought increased rainfall to the Sahara, Arabia, and south and east Asia. After 6 ka, as July insolation decreased, simulated temperatures over the land decreased, the monsoonal winds and rainfall weakened, the northern subtropical deserts expanded, and the present climatic patterns developed. In the southern tropics the changed insolation (more in July, less in January) had exactly the opposite effect. It produced decreased seasonality and less intense summer rains in tropical South America, southern Africa, and Australia. However, the smaller size of the southern continents, especially Australia, muted this effect.

*Paleoclimatic data.* At 18 ka, the pollen data show that the extent of forests in the Atlas Mountains and west Africa was greatly reduced, while dry steppe vegetation occupied the Mediterranean area, which suggests that northwest Africa and the lands around the Mediterranean were cooler than they are today with moisture levels similar to present levels or slightly drier (Fig. 4). This interpretation is in conflict with evidence for high lake levels in the Near East and for greater runoff from the Atlas into the northern Sahara. Most lakes were dry (or low) in the southern Sahara and eastern Africa, indicating that the differences in precipitation from the present were only minor. Weaker monsoonal upwelling and weaker monsoon southwesterlies are indicated by the decreased abundance of *G. bulloides* and windblown pollen in the western Arabian Sea (*47*).

Snowline and paleovegetation data from Australia, New Guinea, New Zealand, and South America for 18 to 15 ka suggest that mean temperatures were 4° to 6°C lower than they are today (*48–51*). Tropical rain forests were reduced because of dry conditions (*48, 49*), and dune fields in central Australia were active (*52*). Only in parts of the southern Andes does the pollen record imply that effective precipitation was greater than it is today (*53*).

From about 12 to 6 ka, the pollen and lake-level data reveal that effective moisture was greater than it was before across northern Africa and down to at least 16°S in eastern Africa, and eastward through Arabia and Afghanistan into northwest India and China.

Crocodiles and hippopotamuses extended their range into the present-day Sahara desert, and people settled near the freshwater lakes (*43*). In China forests expanded at this time because of wetter conditions, and lake levels rose on the Tibetan Plateau (Xizang) and in western China (*54*). In the western Arabian Sea, the increased abundance of G. *bulloides* and windblown pollen from eastern Africa clearly indicate that both monsoonal upwelling and monsoon southwesterlies were stronger (*47*). All of this evidence points to a major strengthening of the north African–Asian monsoon coincident with the period of increased seasonality of solar radiation in the Northern Hemisphere (*55, 56*). After 6 ka the northern tropical lake levels fell as would be expected with the return of solar radiation to modern values (Fig. 2).

For the Southern Hemisphere between 9 and 6 ka the mesic forests reached their maximum extent in Australia, New Guinea, New Zealand, and parts of tropical and temperate South America, although at 30° to 35°S in South America pollen data indicated that conditions were drier (*57*). By 6 ka the levels of Lake Titicaca (16°S) and most other lakes were lower than levels today (*58, 59*).

*Data-model comparisons*. The observations clearly portray the intensified monsoons in northern Africa and southern Asia from about 12 to 6 ka in contrast to the weaker monsoons of glacial and present times. For tropical lands, this is the outstanding feature of the 18,000-year climatic record. Our simulation experiments indicate a pattern of intensified northern monsoon circulation and precipitation that agrees closely in time and space with the observations and explains the phenomenon in terms of orbitally induced change in solar radiation.

To illustrate this broad agreement of observations and simulations, we have made a quantitative comparison between the observed record of changes in level of closed-basin lakes in the northern tropics and the model's simulation of precipitation-minus-evaporation (Fig. 6) (*8*). We compared these two independent estimates of the surface hydrologic budget for each 3000-year interval from 18 ka to the present. This period covers essentially one precession cycle from near present insolation values around 18 ka to the greatly increased summer insolation of 9 ka to the present (Fig. 2). For the period 12 to 6 ka the model simulates a 25 to 30% increase in rainfall compared to present values, and about a sevenfold increase in net moisture availability as measured by precipitation-minus-evaporation (Fig. 6). For comparison, most northern tropical closed-basin lakes in our survey were at intermediate or high levels between 12 and 6 ka, whereas almost all are at low levels now (Fig. 6). Similar estimates of increased rainfall and precipitation-minus-evaporation are available from paleohydrologic studies based on field data (*60*). This agreement between model results and geologic data appears in large part to answer one of the long-standing puzzles posed in the introduction.

Outside of the northern tropics, our data sets are not as complete in time and space, and we have not made regional comparisons of the type shown in Figs. 5 and 6. We have compared the simulations and observations at selected locations and there are areas and times of agreement and disagreement, some of which are cited as examples below.

For the Southern Hemisphere, the simulated strengthening of the southern westerlies over the eastern South Pacific and southern South America for 18 ka is supported by pollen data from southern Chile (*53*). For 9 ka the model indicates that seasonality and summer rains decreased, and the pollen and lake-level evidence for subtropical South America, South Africa, and Madagascar supports this reconstruction. However, elsewhere in the tropical and temperate latitudes of South America (*53, 61*), Australia (*62*), and New Zealand (*50*) the pollen data show that mesic forests were at their maximum extent, which suggests that conditions were moister than those simulated by the model.

The simulated climate disagrees with some geologic data concerning the time of the onset of enhanced northern monsoon rains. The model indicates that the onset occurred at 15 ka, whereas the data show that lake levels did not rise until around 12 ka (Fig. 6). We do not know the reason for this discrepancy, but perhaps glacial-age aerosols significantly depleted the incoming solar radiation in the tropics, a factor not included in our model.

Another area of apparent disagreement for the last glacial maximum (18 ka) between the geologic data and the simulations of our model and other models (*18*) centers around New Guinea. There, glacier equilibrium lines and vegetation zones were about 1000 m lower than at present at some time during the last glacial interval (*49*); this evidence implies that terrestrial temperatures were 5° to 7° lower then, whereas adjacent sea-surface temperatures were only about 2°C lower (*5*). Only about a third to a half of the implied terrestrial cooling is simulated by the model, in which sea-surface temperature estimates from marine plankton are a surface boundary condition (*63–65*). The same type of disagreement occurs in other areas of tropical mountain glaciation, including eastern Africa and the central Andes (*51, 66*). The model's simulation of a weakened Indian monsoon is consistent, however, with the observed decrease in the upwelling indicated by the G. *bulloides* in the western Arabian Sea.

In the Mediterranean region at 18 ka, the paradox of high lake levels in northwest Africa and the Near East coinciding with pollen evidence for steppe vegetation may be explained by the model simulation of a southward shift of the westerlies in summer. Such a shift would have brought cloudiness, occasional rains, and low evaporation rates into the region and would have reduced the strength of the summer subtropical high that prevails there today. Winters would have been cold and precipitation reduced because of strong northeasterly airflow.

## Causes and Mechanisms of Long-Term Change

Our modeling experiments show how orbitally induced changes in insolation and variations in surface boundary conditions affect regional climates and thus help answer the questions posed in the introduction by explaining the major shifts in vegetation, marine plankton, and hydrologic budgets. Variations in insolation changed the seasonality of climate in the tropics and mid-latitudes. By enhancing the thermal contrast between oceans and land, increased seasonality produced strong summer monsoons from 12 to 6 ka in the Northern Hemisphere tropics and subtropics and warm and dry summers in the continental interiors of northern mid-latitudes. Lake-level data agree with these results. Lakes expanded in the Sahara and elsewhere in the northern tropics, but lake levels were low in central and western North America (Figs. 3 and 4). Pollen data and their derived climate estimates also indicate that the climate was warm and dry in central North America and Europe. The model output suggests that in the Southern Hemisphere the orbital variations produced somewhat weaker summer monsoons in Africa and South America at 9 ka, although more data from southern Africa and southern Amazonia are needed to assess this interpretation.

The model results indicate how surface boundary conditions (ice-sheet size, sea-ice extent, and sea-surface temperatures), themselves representing a delayed response to radiation changes, could have influenced atmospheric circulation patterns and thus the patterns in temperature and precipitation that affect vegetation. The extent of sea ice in the North Atlantic, which is largely controlled by cold northwesterly winds from the North American ice sheet, in turn

influenced the location and strength of the westerly jet stream over western Europe. The North American ice sheet at its maximum extent split the westerly jet stream over North America and decreased the seasonality of climate in eastern North America. Both the North American and Eurasian ice sheets produced anticyclones that led to surface easterly winds along their southern boundaries. The southward-displaced jet stream and storm track at 18 ka led to high lake levels in the American Southwest, and the surface easterlies along the ice-sheet edge produced dry conditions in the Northwest. The climates of North America from 18 to 12 ka were unlike any today, and this condition led to floras and faunas without analogs in today's vegetation and animal communities. The radiation maximum occurred before 9 ka and resulted in high temperatures to the southwest of the Laurentide ice sheet. In contrast, in eastern North America the slow retreat of the ice sheet delayed the summertime thermal maximum until 6 ka.

Climate models provide useful thermodynamical and dynamical explanations for the past patterns in the data. Paleoclimatic data in turn indicate that climate models have fair skill in simulating the broad geographic patterns of atmospheric circulation, temperature, and moisture. The stage is now set for new paleoclimatic experiments with versions of the models that include additional interactive components of the climate system, for example, soil moisture, ocean circulation, aerosol content, and other factors (*67, 68*). New paleoclimatic tests of the model results are also needed. These can build on results described here and will show how well the models can simulate the geographic patterns of vegetation, lakes, and marine plankton for each new model experiment.

## Implications for Understanding Past and Future Changes

As confidence is gained in the climate and ocean models, opportunities will arise both at global and regional scales to examine the effects of climatic change on biosphere dynamics. For example, if the changing distributions of spruce, oak, and other trees in North America and Europe can be understood in terms of the climate simulated by the model, then key paleoecological problems, such as the potential for migrational lags in plant distributions, can be examined in a new light (*69*). Similarly, we can evaluate in the marine data the extent to which the distribution of certain foraminiferal species can be related to distinct oceanic conditions (for example temperature and nutrient levels) that reflect climatic change. Most importantly, the physical mechanisms responsible for these environmental and biospheric changes can be better understood.

Climate has influenced human activities. Two great cultural developments emerged at about the time of major environmental change between 12 and 10 ka—the earliest appearance of agriculture in the Old World, and the cultural changes accompanying extinction of the Pleistocene megafauna in the New World. Both developments may have been caused at least indirectly by the types of climatic change examined here. Now we may be faced with the reverse: human modification of climate and of related aspects of the physical environment. Application of a well-tested climate model is at present the only method for predicting these climatic and environmental changes and can help in planning a response to them. COHMAP research is contributing to the testing of these models and to the understanding of past climates.

### REFERENCES AND NOTES


1. J. Croll, *Philos. Mag.* **28**, 121 (1864); M. Milankovitch, *K. Serb. Akad. Geogr. Spec. Publ.* **132**, 1 (1941), translated by Israel Program for Scientific Translations, Jerusalem (U.S. Department of Commerce, Washington, DC, 1969).
2. A. L. Berger, *Quat. Res. (New York)* **9**, 139 (1978).
3. See J. Imbrie and K. P. Imbrie *Ice Ages: Solving the Mystery* (Enslow, Short Hills, NJ, 1979) for historical essay on the development of the theory.
4. J. D. Hays, J. Imbrie, N. J. Shackleton, *Science* **194**, 1121 (1976).
5. Climate Mapping and Prediction: CLIMAP Project Members, *ibid.* **191**, 1131 (1976); *Geol. Soc. Am. Map Chart Ser. MC-36* (1981).
6. W. L. Gates, *Science* **191**, 1138 (1976); *J. Atmos. Sci.* **33**, 1844 (1976); S. Manabe and D. G. Hahn, *J. Geophys. Res.* **82**, 3889 (1977).
7. J. E. Kutzbach *et al.*, Eds., *Global Climates for 9000 and 6000 Years Ago* (Univ. of Minnesota Press, Minneapolis, in press).
8. J. E. Kutzbach and F. A. Street-Perrott, *Nature* **317**, 130 (1985).
9. M. G. Winkler, A. M. Swain, J. E. Kutzbach, *Quat. Res. (New York)* **25**, 235 (1986); G. L. Jacobson, T. Webb III, E. C. Grimm, in *North America and Adjacent Oceans During the Last Glaciation*, W. F. Ruddiman and H. E. Wright, Jr., Eds. (Geological Society of America, Boulder, CO, 1987), pp. 277–288.
10. B. Huntley and H. J. B. Birks, *An Atlas of Past and Present Pollen Maps for Europe 0–13,000 Years Ago* (Cambridge Univ. Press, Cambridge, 1983).
11. P. J. Bartlein and T. Webb III, *Syllogeus* **55**, 301 (1985).
12. T. Webb III, P. J. Bartlein, J. E. Kutzbach, in *North America and Adjacent Oceans During the Last Glaciation*, W. F. Ruddiman and H. E. Wright, Jr., Eds. (Geological Society of America, Boulder, CO, 1987), pp. 447–462.
13. C. W. Barnosky, P. M. Anderson, P. J. Bartlein, *ibid.*, pp. 289–321.
14. Early experiments for 18 ka (*15*) were followed by those of Gates and of Manabe and Hahn (*6*), who were able to use the initial CLIMAP estimates of glacial-age boundary conditions to simulate the contemporaneous circulation, and by those of Broccoli and Manabe (*16*) and of Rind and Peteet (*17*), who used the final CLIMAP estimates. More recent comprehensive simulations of the climate of 18 ka have been produced with coupled atmosphere-ocean models (*18*), and Barron (*19*) completed a series of simulations of Cretaceous climates.
15. J. Williams, R. G. Barry, W. M. Washington, *J. Appl. Meteorol.* **13**, 305 (1974).
16. A. J. Broccoli and S. Manabe, *Clim. Dyn.* **1**, 87 (1987).
17. D. Rind and D. Peteet, *Quat. Res. (New York)* **24**, 1 (1985).
18. S. Manabe and A. J. Broccoli, *J. Geophys. Res.* **90**, 2167 (1985).
19. E. Barron, in *Paleoclimate Analysis and Modeling*, A. D. Hecht, Ed. (Wiley, New York, 1985), pp. 397–421.
20. E. J. Pitcher *et al.*, *J. Atmos. Sci.* **40**, 580 (1983); V. Ramanathan, E. J. Pitcher, R. C. Malone, M. L. Blackmon, *ibid.*, p. 605.
21. The model incorporates atmospheric dynamics based on the equations of motion, and it includes radiative and convective processes, condensation, and evaporation. It has nine vertical levels and a spectral representation to wave number 15 of the horizontal fields of wind, temperature, pressure, and moisture. The spectral representation equates to a horizontal resolution of about 4° latitude and 7.5° longitude. The model was typically run for 450 simulated days for each July and January at each 3000-year interval. The 450-day history was then divided into three 150-day segments. For sampling purposes the first 60 days of each segment were ignored, and three 90-day averages were obtained and combined to form a 90-day ensemble average that was compared to a control simulation, represented by the similarly constructed ensemble average for today. The six independent 90-day averages, three from each experiment and three from the control, were used to estimate the model's natural variability and to assess the statistical significance of the simulated climatic changes (*22*). A series of multiyear experiments for the present and for 9 ka with full seasonal cycles (365 days per year) was used to check that our conclusions on the basis of July and January simulations (*23–25*) were similar to our conclusions on the basis of full-year simulations (*24, 26*). We were also able to estimate the annual-average climatic changes by weighting the January and July results according to the changing length of the months for the different orbital configurations.

    We prescribed solar radiation according to changes determined from orbital parameters (*2*) (Fig. 2). Recent measures from ice cores provided estimates of changing atmospheric $CO_2$ concentrations and changing atmospheric aerosol concentration (*27*). Our experiments included one with reduced $CO_2$ concentration at 18 ka, but this potential climate feedback mechanism has been studied more extensively by Broccoli and Manabe (*16*). We have not yet performed model experiments to assess the effects of changed aerosol concentrations. Descriptions of the other paleoclimatic boundary conditions appear in (*25, 28*), and full descriptions of the model results are published elsewhere (*7, 8, 13, 25, 29, 30*).
22. R. M. Chervin and S. H. Schneider, *J. Atmos. Sci.* **33**, 405 (1976).
23. J. E. Kutzbach, *Science* **214**, 59 (1981).
24. ——— and B. Otto-Bliesner, *J. Atmos. Sci.* **39**, 17 (1982).
25. J. E. Kutzbach and P. J. Guetter, *ibid.* **43**, 1726 (1986).
26. J. E. Kutzbach and R. Gallimore, *J. Geophys. Res.* **93**, 803 (1988); J. F. B. Mitchell, N. S. Grahame, K. J. Needham, *ibid.*, p. 8283.
27. J. M. Barnola, D. Raynaud, Y. S. Korotevitch, C. Lorius, *Nature* **329**, 408 (1987).
28. For the glacial maximum of 18 ka the estimates of surface boundary conditions that we used were originally compiled by CLIMAP (*5*). These include (i) ice-sheet location and thickness, (ii) sea-ice extent, (iii) sea-surface temperature, (iv) land albedo, and (v) changed continental margins resulting from lower sea level. For the 12 ka simulation, most parameters were changed about halfway toward modern values, and for the 9 ka simulation all but the size of the Laurentide ice sheet were set at modern values (Fig. 2). COHMAP marine data are concentrated in the North Atlantic and equatorial Atlantic oceans and the Arabian Sea (Fig. 1), where sedimentation rates were high enough to record large-scale changes over 3000-year intervals. For 18 and 15 ka we used the extensive marine core data of CLIMAP (*5*) to fix the glacial-age sea-surface temperatures (Fig. 2).
29. W. L. Prell and J. E. Kutzbach, *J. Geophys. Res.* **92**, 8411 (1987).
30. J. E. Kutzbach and H. E. Wright, Jr., *Quat. Sci. Rev.* **4**, 147 (1985); J. E. Kutzbach, in *North America and Adjacent Oceans During the Last Glaciation*, W. F. Ruddiman and H. E. Wright, Jr., Eds. (Geological Society of America, Boulder, CO, 1987), pp. 425–446.

31. A. Berger *et al.*, Eds., *Milankovitch and Climate* (Reidel, Dordrecht, 1986).
32. F. A. Street-Perrott and N. Roberts, in *Variations in the Global Water Budget*, F. A. Street-Perrott, M. A. Beran, R. A. S. Ratcliffe, Eds. (Reidel, Hingham, MA, 1983), pp. 331–345.
33. T. R. VanDevender, R. S. Thompson, J. L. Betancourt, in *North America and Adjacent Oceans During the Last Glaciation*, W. F. Ruddiman and H. E. Wright, Jr., Eds. (Geological Society of America, Boulder, CO, 1987), pp. 323–352; W. G. Spaulding and L. J. Graumlich, *Nature* **320**, 441 (1986).
34. N. G. Kipp, *Geol. Soc. Am. Mem.* **146**, 3 (1976).
35. W. F. Ruddiman and H. E. Wright, Jr., Eds. *North America and Adjacent Oceans During the Last Deglaciation* (Geological Society of America, Boulder, CO, 1987).
36. J. Imbrie and J. Z. Imbrie, *Science* **207**, 943 (1984); J. Imbrie *et al.*, in *Milankovitch and Climate*, A. Berger, J. Imbrie, J. Hays, G. Kukla, B. Saltzmann, Eds. (Reidel, Dordrecht, 1986), pp. 269–305.
37. T. Webb III, *Vegetatio* **69**, 177 (1987).
38. B. Huntley, in *Vegetation History*, B. Huntley and T. Webb III, Eds. (Junk, Dordrecht, in press).
39. M. B. Davis, R. W. Spear, L. C. K. Shane, *Quat. Res. (New York)* **14**, 240 (1980); B. Huntley and I. C. Prentice, *Science* **241**, 687 (1988).
40. P. J. Bartlein, T. Webb III, E. C. Fleri, *Quat. Res. (New York)* **22**, 361 (1984).
41. J. C. Ritchie, L. C. Cwynar, R. W. Spear, *Nature* **305**, 126 (1983).
42. The wind-scoured ridges, sand dunes, and loess deposits in the Great Plains that were presumably produced at this time can be attributed to strong seasonal northwest winds, whereas the prevailing anticyclonic winds from the east controlled the hydrological and vegetational development (*30*).
43. F. A. Street and A. T. Grove, *Quat. Res. (New York)* **12**, 83 (1979); F. A. Street-Perrott and S. P. Harrison, in *Paleoclimate Analysis and Modeling*, A. D. Hecht, Ed. (Wiley, New York, 1985), pp. 291–340.
44. B. Huntley and I. C. Prentice, in *Global Climates for 9000 and 6000 Years Ago*, J. E. Kutzbach *et al.*, Eds. (Univ. of Minnesota Press, Minneapolis, in press).
45. J. S. Fein and P. L. Stephens, Ed., *Monsoons* (Wiley, New York, 1987).
46. A region of lower pressure over the warmer waters of the western Indian Ocean led to increased rainfall over parts of east and northeast Africa. Rainfall was less than at present over southern Asia because the combination of a warmer-than-present western Indian Ocean and a colder-than-present Asian continent served to weaken the Asian monsoon.
47. E. Van Campo, J.-C. Duplessy, M. Rossignol-Strick, *Nature* **296**, 56 (1982); W. L. Prell and E. Van Campo, *ibid.* **323**, 576 (1986).
48. A. P. Kershaw, in *Ecological Biogeography of Australia*, A. Keast, Ed. (Junk, The Hague, 1981), pp. 83–101; D. Walker and G. Singh, in *Australian Vegetation*, R. H. Groves, Ed. (Cambridge Univ. Press, Cambridge, 1981), pp. 26–43.
49. G. S. Hope and J. A. Peterson, in *The Equatorial Glaciers of New Guinea*, G. S. Hope, J. A. Peterson, I. Allison, U. Radok, Eds. (Balkema, Rotterdam, 1976), pp. 173–205.
50. B. P. Pillans, W. A. Pullar, M. J. Selby, J. M. Soons, in *Landforms of New Zealand*, J. M. Soons and M. J. Selby, Eds. (Longman's Aukland, 1982), pp. 15–54; M. S. McGlone and W. W. Topping, *N.Z. J. Bot.* **21**, 53 (1983); N. T. Moar, *N.Z. J. Ecol.* **3**, 4 (1980); M. S. McGlone and J. L. Bathgate, *N.Z. J. Bot.* **21**, 292 (1983).
51. C. M. Clapperton, *Quat. Sci. Rev.* **2**, 83 (1983); J. H. Mercer, *Annu. Rev. Earth Planet. Sci.* **11**, 99 (1983).
52. R. J. Wasson, *Z. Geomorphol. Suppl.* **45**, 85 (1983).
53. C. Villagran, *VII Simposio Argentio de Paleobotanica y Palinologia Actas*, Buenos Aires (1987), p. 133; C. J. Heusser, *Proceedings of the American Quaternary Association 8th Biennial Meeting* (1984), p. 59.
54. M. G. Winkler and P. K. Wang, in *Global Climates for 9000 and 6000 Years Ago*, J. E. Kutzbach *et al.*, Eds. (Univ. of Minnesota Press, Minneapolis, in press).
55. At both 9 and 6 ka, the Near East marks the northern limit of the area of monsoonal influence (*56*), with the southern part (for example, Arabia) receiving enhanced tropical precipitation (higher lake levels) but the northern part (Iran, Anatolia) experiencing greater aridity than at present (low lake levels and percentages of tree pollen). This feature is also simulated correctly by the increased dry northeasterly winds on the western side of the south Asian summer-monsoon low.
56. N. Roberts and H. E. Wright, Jr., in *Global Climates for 9000 and 6000 Years Ago*, J. E. Kutzbach *et al.*, Eds. (Univ. of Minnesota Press, Minneapolis, in press).
57. C. J. Heusser, *Science* **220**, 1429 (1983); H. L. D'Antoni, *Quat. S. Am. Antarct. Peninsula* **1**, 83 (1983); M. A. Gonzalez, *VII Congr. Geol. Argent. Actas* **3**, 411 (1981).
58. R. H. Galloway, V. Markgraf, J. P. Bradbury, *J. S. Am. Earth Sci.*, in press.
59. D. Wirrman and L. F. DeOliveira Almeida, *Palaeogeogr. Palaeoclimatol. Palaeoecol.* **59**, 315 (1987).
60. J. E. Kutzbach, *Quat. Res. (New York)* **14**, 210 (1980); S. Hastenrath, and J. E. Kutzbach, *ibid.* **19**, 141 (1983); A. M. Swain, J. E. Kutzbach, S. Hastenrath, *ibid.*, p. 1. The model simulated a 25 to 30% increase in rainfall between about 12 and 6 ka, and, with a lake-hydrology submodel, we estimated that this could represent a sevenfold expansion of the fractional area covered by closed-basin lakes.
61. B. C. S. Hansen, H. E. Wright, Jr., J. P. Bradbury, *Geol. Soc. Am. Bull.* **95**, 1454 (1984); C. J. Heusser, in *Late Cainozoic Palaeoclimates of the Southern Hemisphere*, J. C. Vogel, Ed. (Balkema, Rotterdam, 1984), pp. 59–64; V. Markgraf, *Palynology* **7**, 43 (1983); V. Markgraf, in *Global Climates for 9000 and 6000 Years Ago*, J. E. Kutzbach *et al.*, Eds. (Univ. of Minnesota Press, Minneapolis, in press).
62. J. R. Dodson, P. W. Greenwood, R. L. Jones, *J. Biogeogr.* **13**, 357 (1986); V. Markgraf, J. P. Bradbury, J. Busby, *Palaios* **1**, 368 (1986); R. M. Binder and A. P. Kershaw, *Search* **9**, 44 (1978); J. M. Bowler, *Hydrobiologia* **82**, 431 (1981).
63. It has been suggested (*17, 64*) that the sea-surface temperature estimates are too warm. New data and analysis confirm the earlier estimates, however (*65*). This potential discrepancy between land and sea remains to be resolved.
64. P. Webster and N. Streten, *Quat. Res. (New York)* **10**, 279 (1978).
65. D. M. Anderson, N. J. Barratt, W. L. Prell, *Eos* **68**, 333 (1988).
66. S. Hastenrath, *Z. Gletscherkunde Glazialgeol.* **21**, 183 (1985).
67. Several general circulation modeling experiments provide valuable insights into key physical interactions in the climatic system. Effects of increasing $CO_2$ have been widely investigated. Manabe and Broccoli (*18*) isolated the climate effects uniquely attributable to Northern Hemisphere ice sheets, and Broccoli and Manabe (*16*) studied the respective roles of ice sheets, atmospheric $CO_2$, and land albedo. Others (*68*) evaluated the effects of land albedo, ice elevation, cold sea-surface temperatures, and sea ice in the North Atlantic Ocean on Northern Hemisphere atmospheric circulation.
68. D. Rind, D. Peteet, W. Broecker, A. McIntyre, W. F. Ruddiman, *Clim. Dyn.* **1**, 3 (1986); D. Rind and D. Peteet, *Climatic Change* **9**, 357 (1986); S. H. Schneider, *ibid.*, p. 361; D. Rind, *J. Geophys. Res.* **92**, 4241 (1987).
69. M. B. Davis, *Vegetatio.* **67**, i (1986); I. Prentice, *ibid.*, p. 131.
70. G. H. Denton and T. S. Hughes, *The Last Great Ice Sheets* (Wiley, New York, 1980).
71. J. R. Petit, M. Briat, A. Royer, *Nature* **293**, 391 (1981); L. G. Thompson and E. Moseley-Thompson, *J. Volcanol. Geotherm. Res.* **11**, 11 (1981).
72. A. Neftel *et al.*, *Nature* **295**, 220 (1982); C. Lorius, D. Raynaud, J. R. Petit, J. Jousel, L. Merlivat, *Ann. Glaciol.* **5**, 88 (1984).
73. The left-hand (data) panels of Figs. 3 and 4 were compiled from a variety of published and unpublished sources. The principal data sources and author responsibilities are listed below. Ice sheets and paleogeography data are in (*70, 74*); A. S. Dyke and V. K. Prest, *Geogr. Phys. Quat.* **41**, 237 (1987); D. M. Hopkins, in *Paleoecology of Beringia*, D. M. Hopkins, J. V. Matthews, Jr., C. E. Schweger, S. B. Young, Eds. (Academic Press, New York, 1982), pp. 3–28. Local modifications of the basic patterns were made by P. M. Anderson (Alaska), H. E. Wright, Jr. (eastern North America), W. F. Ruddiman (paleo-oceanography), and B. Huntley (European paleogeography); sea ice data are from (*5, 70*); modifications of the basic patterns were made by W. F. Ruddiman. European pollen data are in (*10*); additional data were compiled by B. Huntley. North American pollen data are in (*37*); additional data were compiled by P. M. Anderson and L. B. Brubaker (Alaska) and J. C. Ritchie (northwestern Canada). North Atlantic foraminiferal data were compiled by B. Molfino and W. F. Ruddiman. Present precipitation data are from A. Baumgartner and E. Reichel [*The World Water Balance* (Elsevier, Amsterdam, 1975)]. The data forming the basis of relative moisture patterns were compiled from published and unpublished sources, including paleoecological data (fossil-pollen data from lakes and bogs, plant-macrofossil data from the fossilized middens of pack rats), and geomorphologic and sedimentologic evidence of the former lake levels. The compiled data were subjectively interpreted in terms of moisture status (relative to present conditions) and assigned three categories: wetter than present, drier than present, and no change from present (including data that were indeterminate or ambiguous). Authors responsible for individual regional compilations include: western North America, R. S. Thompson (fossil pollen and plant macrofossil data), C. W. Barnosky (pollen data), W. G. Spaulding (plant macrofossil data), and S. P. Harrison (lake-level data); Africa and Asia, F. A. Street-Perrott and N. Roberts (African and Middle eastern lake levels and pollen), G. M. Peterson (Soviet pollen), and M. G. Winkler and P. K. Wang (east Asian pollen and lake levels); Australia, J. Dodson and S. P. Harrison (pollen and lake levels), M. S. McGlone (New Zealand pollen).
74. A. A. Velichko, H. E. Wright, Jr., C. W. Barnosky, *Late Quaternary Environments of the Soviet Union* (Univ. of Minnesota Press, Minneapolis, 1984).
75. Grants from the National Science Foundation (NSF) (Climate Dynamics Program) and the Department of Energy (Carbon Dioxide Research Division) provided the major support for this project. Additional support for COHMAP was provided by the Nuclear Regulatory Commission to NSF. The specific grant numbers are: NSF/ATM-8713981 and DOE FG02-85ER60304 (Brown University), NSF/ATM87-13979 (Lamont Doherty Geological Observatory of Columbia University), NSF/ATM-8714122 (University of Minnesota), NSF/ATM-8713980 (University of Oregon), NSF/ATM-8713227 and NSF/ATM-8603295 (University of Wisconsin–Madison). The numerical climate model simulations were made at the NSF-sponsored National Center for Atmospheric Research, Boulder, CO, with computing grant 35381017. We thank many other collaborators and colleagues, including K. Anderson, S. Bottema, R. A. Bryson, R. Chervin, K. Gajewski, R. Gallimore, D. C. Gaudreau, E. C. Grimm, S. Hastenrath, S. E. Howe, J. Jones, P. Klinkman, P. Manesis, B. Molfino, P. Newby, B. Otto-Bliesner, J. T. Overpeck, S. H. Schneider, L. C. K. Shane, M. Sternitzky, R. Steventon, A. Swain, W. Washington, R. S. Webb, and M. Woodworth, the administrative coordinator for COHMAP. We thank the anonymous reviewers for their helpful comments.